Blood First Edition Paper, prepublished online May 9, 2018; DOI 10.1182/blood-2018-01-830901

Warfarin and vitamin K epoxide reductase: a molecular accounting for observed inhibition

Running head: VKOR: structure and warfarin inhibition

Sangwook Wu[1,3,4], Xuejie Chen[2,4], Da-Yun Jin[2], Darrel W. Stafford[2],
Lee G. Pedersen[3*] & Jian-Ke Tie[2*]

[1]Department of Physics, Pukyong National University, Busan, 608-737, South Korea
[2]Department of Biology, University of North Carolina at Chapel Hill, Chapel Hill, NC 27599
[3]Department of Chemistry, University of North Carolina at Chapel Hill, Chapel Hill, NC 27599
[4]These authors contributed equally to this work

Correspondence: Lee G. Pedersen, Department of Chemistry, University of North Carolina at Chapel Hill, Chapel Hill, NC 27599, Tel: 919-962-1578, E-mail: pedersen@ad.unc.edu.

Jian-Ke Tie, Department of Biology, University of North Carolina at Chapel Hill, Chapel Hill, NC 27599, Tel: 919-962-2267, E-mail: jktie@email.unc.edu

Word count for text:	4184
Word count for abstract:	248
Figure/table count:	7
Reference count:	57
Scientific category:	Thrombosis and Hemostasis

Key Points:

- Warfarin reversibly inhibits VKOR by forming a T-shaped stacking interaction with residue Y139 of the proposed TYA warfarin-binding motif
- Warfarin-resistant non-bleeding phenotype for patients bearing VKOR mutations explained by MD simulation and cell-based functional study

Abstract

Vitamin K epoxide reductase (VKOR), an endoplasmic reticulum membrane protein, is the key enzyme for vitamin K-dependent carboxylation, a post-translational modification that is essential for the biological functions of coagulation factors. VKOR is the target of the most widely prescribed oral anticoagulant warfarin. However, the topological structure of VKOR and the mechanism of warfarin's inhibition of VKOR remain elusive. Additionally, it is not clear why warfarin-resistant VKOR mutations identified in patients significantly decrease warfarin's binding affinity, but have only a minor effect on vitamin K binding. Here, we used immunofluorescence confocal imaging of VKOR in live mammalian cells and PEGylation of VKOR's endogenous cytoplasmic-accessible cysteines in intact miscrosomes to probe the membrane topology of human VKOR. Our results show that the disputed loop sequence between the first and second transmembrane (TM) domain of VKOR is located in the cytoplasm, supporting a three-TM topological structure of human VKOR. Using molecular dynamics (MD) simulations, a T-shaped stacking interaction between warfarin and tyrosine residue 139, within the proposed $TY_{139}A$ warfarin-binding motif, was observed. Furthermore, a reversible dynamic warfarin binding-pocket opening and conformational changes were observed when warfarin binds to VKOR. Several residues (Y25, A26, and Y139) were found essential for warfarin binding to VKOR by MD simulations, and these were confirmed by the functional study of VKOR and its mutants in their native milieu using a cell-based assay. Our findings provide new insights into the dynamics of the binding of warfarin to VKOR, as well as into warfarin's mechanism of anticoagulation.

Introduction

Warfarin, a coumarin derivative, was originally used as a rodenticide in 1948. Due to its promise for preventing thromboembolic disorders, warfarin was approved as a medication in 1954, and has remained the mainstay of anticoagulation therapy[1,2]. More than 30 million prescriptions for warfarin are written annually in the United States alone[3]. Despite its effectiveness and widespread use, warfarin is also ranked among the top ten medications with serious adverse drug events due to its narrow therapeutic index and the broad individual variability of dosing requirements[4]. In the past decade, several novel oral anticoagulants that directly target thrombin and Factor Xa have been advocated as warfarin replacements. However, the cost of these drugs, the challenges of reversing their anticoagulation effects, and the severe bleeding and ischemic stroke problems they can cause, continue to make warfarin the choice of most physicians[5].

Warfarin impairs the biosynthesis of functional vitamin K-dependent proteins by the inhibition of vitamin K epoxide reductase (VKOR). This action limits the production of carboxylated vitamin K-dependent proteins that control blood coagulation, vascular calcification, bone metabolism, and other important physiological processes[6]. Site-direct mutagenesis studies show that cysteines 132 and 135 comprise a $C_{132}XXC_{135}$ active site redox center of VKOR[7,8]. Based on multiple sequence alignments[9] and functional studies of the naturally occurring warfarin-resistant mutations at residue Y139[10], the $TY_{139}A$ sequence has been proposed as part of the warfarin-binding site[9-11].

VKOR is an integral endoplasmic reticulum (ER) membrane protein. Like other membrane proteins, structure and function studies of VKOR have been challenging, and the results of these studies are often controversial[12]. Our current understanding of VKOR's structure is based on biochemical studies of the membrane topology of human VKOR[13-15], on the X-ray crystal structure of a VKOR bacterial (*Synechococcus*) homologue (*Syn*-VKOR)[16], and on computer-aided molecular

dynamics (MD) simulations of human VKOR[17,18]. Both three- and four-transmembrane (TM) topology models for human VKOR have been proposed. While there is no doubt that the $C_{132}XXC_{135}$ redox motif is VKOR's active site, the role of two other conserved cysteines (C43 and C51) remains controversial[14,16,19].

The mechanism of how and where warfarin binds to VKOR is also unclear. Both irreversible[20,21] and reversible[22] inhibition mechanisms have been proposed for warfarin inhibition of VKOR. As a reversible inhibitor, warfarin appears to inhibit VKOR in a noncompetitive manner[23,24]. However, a recent study suggests that warfarin competitively inhibits VKOR by competing with vitamin K[25]. Several studies modeling warfarin's action within model structures of VKOR have identified residues that potentially interact with warfarin[25,26]. However, no direct interaction between warfarin and the experimentally supported $TY_{139}A$ warfarin-binding motif has been observed. It is worth noting that these modeling studies used a four-TM topology model of human VKOR, derived from the crystal structure of *Syn*-VKOR, which appears to have a different topological structure from human VKOR[14]. Therefore, the mechanism of warfarin inhibition of human VKOR at the molecular level remains elusive.

In this study, we re-probed the topological structure of human VKOR using immunofluorescence confocal imaging and a recently introduced approach for determining membrane protein topology[27,28]. We also employed a conventional all-atom MD simulation and a steered MD simulation to model the dynamic nature of warfarin binding to the three-TM human VKOR structure. Results from the current study provide new insights into how warfarin binds to human VKOR within the context of the dynamics of the enzyme.

Methods

Materials and plasmid constructions

Mammalian dual expression vector pBudCE4.1, rabbit anti-human VKOR polyclonal antibody (Cat# PA5-60093), AF-488 conjugated donkey anti-mouse IgG (Cat# A21202), and AF-568 conjugated donkey anti-rabbit IgG (Cat# A10042) were purchased from ThermoFisher Scientific (Rockford, IL). Mouse anti-protein disulfide isomerase (PDI) monoclonal antibody (Cat# Ab2792) was from Abcam (Cambridge, MA). Mouse anti-tubulin monoclonal antibody (Cat# A01410) was from GenScript (Piscataway, NJ). Mouse anti-GAPDH monoclonal antibody (Cat#, 60004-1-Ig) was from Proteintech Group, Inc. (Rosemont, IL). mPEG-MAL-5000 was purchased from Laysan Bio Inc. (Arab, AL). QuickChange site-directed mutagenesis kit was from Agilent (Santa Clara, CA). HEK293 and COS-7 cells were from ATCC (Manassas, VA). HEK293 reporter cells with their endogenous VKOR and VKOR-like enzyme (VKORC1L1) knocked out by TALENs-mediated genome editing was described previously[29]. All VKOR mutations were created by a QuickChange mutagenesis kit in pBudCE4.1 mammalian expression vector, as previously described[14].

Immunofluorescence confocal microscopy and cytoplasmic-accessible cysteine PEGylation

To determine the location of the disputed loop sequence of VKOR in live cells, we used immunofluorescence confocal microscopy imaging, as previously described[30]. In brief, human VKOR was transiently expressed in COS-7 cells on coverslips. The cells were washed with phosphate buffered saline solution and fixed with 4% paraformaldehyde. Fixed cells were selectively permeabilized with either 50 μg/mL digitonin or 0.25% Triton X-100. Permeabilized cells were then blocked with 2% bovine serum albumin with 5% fetal bovine serum, and co-stained with primary antibodies. Primary antibody co-staining includes rabbit anti-VKOR with mouse anti-tubulin (cytoplasmic marker) or with mouse anti-PDI (ER luminal marker) antibodies. Immunofluorescence staining was performed with AF-488 conjugated donkey anti-mouse IgG and AF-568 conjugated

donkey anti-rabbit IgG. The cell nuclei were stained with 2 μM Hoechst 33342. Confocal microscopy was performed on a Zeiss LSM710 confocal laser scanning microscope[31].

For PEGylation of the endogenous cytoplasmic-accessible cysteine of VKOR, flag-tagged VKOR or its C43/51A mutant were stably expressed in HEK293 cells. VKOR containing microsomes were prepared and labeled by freshly prepared mPEG-MAL-5000, as previously described[27].

Cell-based functional and enzyme kinetics study of VKOR

The cell-based functional study of VKOR and its mutants was performed in VKOR/VKORC1L1-knockout FIXgla-PC/HEK293 reporter cells, as previously described[29]. VKOR activity was expressed as normalized carboxylated FIXgla-PC. Wild-type VKOR activity was normalized to 100%. Warfarin resistance was evaluated by determining the half-maximal inhibition concentration (IC_{50}) of warfarin. To determine the reversibility of warfarin inhibition of VKOR, FIXgla-PC/HEK293 reporter cells were seeded with different number of cells in the multi-well cell culture plate, and cultured with increasing concentrations of vitamin K epoxide (KO) in the presence and absence of warfarin. Apparent Vmax was determined by a Lineweaver-Burk plot. All data was processed using GraphPad software.

Removal of warfarin from VKOR-warfarin complex

To study the reversibility of warfarin binding to VKOR *in vitro*, VKOR containing microsomes[7] (300 μL) were incubated with 30 μM warfarin on ice for 30 minutes. Then, warfarin was removed by diluting the VKOR-warfarin complex with Tris-HCl buffer (200 mM Tris-HCl, pH 7.4, 150 mM NaCl) containing 4% BSA, and centrifuged at 45,000 rpm, 4 ˚C for 1 hour[32]. VKOR activity of the washed microsomes was determined, as previously described[7].

Molecular dynamics simulations of warfarin binding to VKOR

Molecular dynamics simulations of warfarin binding to VKOR were performed as previously described[17]. We outline simulations as four time-steps in this study (**Supplemental Figure 1** and **Supplemental Table 1**). Step 1, providing an MD-equilibrated three-TM VKOR in lipid and solvent. Step 2, the 40 ns equilibration of warfarin in the ER lumen near a reasonable access point to the interior of VKOR. Step 3, steered MD simulation to move the warfarin molecule into the locality of the proposed warfarin-binding pocket. Step 4, the long (200 ns) MD simulations of three systems: wild-type VKOR, Y139A and A26T mutants with warfarin initially located at the proposed warfarin-binding pocket at the final simulation of step 3. A separate calculation was started for VKOR at 80 ns, with equilibration following the removal of warfarin.

Results

Membrane topology of human VKOR

The current controversial three- and four-TM topology models of human VKOR have consistent orientations in their last two TMs. However, the first TM has opposite orientations which place the large loop sequence on different sides of the ER membrane (**Figure 1A**). Both models have been supported by VKOR topology studies using green fluorescence protein tagging[13,14]. However, fusing a large protein tag to VKOR may perturb VKOR's correct folding and/or membrane targeting. To probe the location of the disputed loop sequence of *unmodified* VKOR in live cells using immunofluorescence confocal imaging, we transiently expressed wild-type human VKOR in COS-7 cells and selectively permeabilized the cell membrane by digitonin so that the VKOR antibody could access only the cytoplasm, but not the ER lumen[14,30]. **Figure 1B** (top panel) shows that VKOR is detected by the VKOR antibody (**Supplemental Note**, Validation of the VKOR antibody) in the digitonin-permeabilized cells, suggesting the cytoplasmic location of the loop sequence; under the

same conditions, the ER lumen marker PDI[30] cannot be detected, indicating that the ER membrane is intact. When the ER membrane is permeabilized by Triton X-100, VKOR is perfectly co-localized with PDI. Probing VKOR and the cytoplasmic marker tubulin[30] under similar permeabilization conditions (**Figure 1B,** bottom panel) further confirmed the cytoplasmic location of the loop sequence. These results strongly suggest that the disputed loop sequence is located in the cytoplasm, which support the three-TM model of VKOR.

The three-TM VKOR is further supported by PEGylation of VKOR's endogenous cytoplasmic-accessible cysteines with a membrane-impermeable thiol-reactive reagent, mPEG-5000[27]. **Figure 1C** shows that two PEGylated VKOR bands are clearly observed (lane 2), suggesting the cytoplasmic location of VKOR's loop cysteines. This is further confirmed by mutating C43 and C51 (retaining ~80% activity, **Figure 1D**) which significantly decreased the two-PEG VKOR adduct (**Figure 1C**, lane 5). These results, consistent with our previous results[14], again support the three-TM model of VKOR. Additionally, VKOR with both C43 and C51 mutated to alanine retains ~80% activity, suggesting that these two cysteines are not required for VKOR's active site regeneration.

MD simulation of warfarin accessing its binding site in VKOR

Based on the significant experimental data and our MD simulation results of comparing the three- and four-TM models of VKOR[17], we performed the MD simulation of warfarin binding to the three-TM VKOR with a reduced active site (**Supplemental Note**, Modeling warfarin binding to active site reduced VKOR) via the ER lumen (**Supplemental Note**, Modeling warfarin binding to VKOR via cytoplasm). We first performed unconstrained conventional MD simulation for 40 ns to equilibrate the initial configuration of VKOR with warfarin near the luminal face of a path that would enable warfarin to locate the proposed $TY_{139}A$ binding motif (**Figure 2A)**. We then employed steered MD simulation[33,34] to enable warfarin accessing its binding site within a reasonable time (448 ps)

(**Supplemental Video**). Warfarin encounters several key residues along the path from the entrance to the putative binding pocket (**Figure 2B**). Residues R12 and F125 initially resist warfarin's access to the inside of VKOR. Then, it encounters L15 and L128, which are essential for holding TM1 and TM3 together to maintain a stable VKOR structure[17]. At the final stage, the side chain of warfarin is placed near the two active site cysteines, and the coumarin moiety located near L105, one of the hydrophobic residues that helps hold TM1 and TM2 together by hydrophobic interaction with L22[17]. Importantly, warfarin, by this path, is located near the proposed $TY_{139}A$ binding motif forming a T-shaped π-π stacking interaction with residue Y139 (**Supplemental Figure 2A**).

Dynamic binding pocket opening when warfarin binds to VKOR

As warfarin accesses its binding site, it encounters several hydrophobic residues that are essential for maintaining VKOR's stable structure. We assume that the interactions between these hydrophobic residues must be weakened in order to allow warfarin to access its binding pocket. To test this hypothesis, we recorded the minimum distance between the paired leucine residues[17] during the 448 ps steered MD simulation. Our results show a dramatic increase in the minimum distance between L15 and L128 at ~160 ps (**Figure 3)**, suggesting the opening of the warfarin-binding pocket in VKOR. Thereafter, warfarin appears to penetrate into the new cavity of VKOR, as evidenced by significant increases in the minimum distances between L15 and L111 (at 400 ps) and L22 and L105 (at 440 ps). At the same time, the minimum distance between L15 and L128 significantly decreases, suggesting the restoration of the opened entrance. This ordered increase and decrease of the minimum distances between the paired leucine residues provides us with a sequential dynamic opening and closing of the warfarin-binding pocket when warfarin binds VKOR.

The phenyl ring of Y139 is essential for stabilizing warfarin binding

To investigate the role of Y139 in warfarin binding, we performed 200 ns unconstrained conventional MD simulation for warfarin binding to VKOR and its Y139A mutant, which has the aromatic ring of Y139 removed. Compared with VKOR, the Y139A mutant shows significantly lower backbone RMSD values during the 200 ns simulation (**Figure 4A)**, suggesting a less distorted architecture. From ~80 ns, the RMSD value of VKOR significantly increases, indicating that VKOR is undergoing a structural distortion as it equilibrates with warfarin. However, the backbone RMSD value for the Y139A mutant decreases prominently after 80 ns, eventually annealing to the value of the reference structure. This result suggests that warfarin rapidly escapes from the Y139A mutant, and that the distortion to VKOR structure is reversible. The reversibility of the VKOR structure deformation was further confirmed by the removal of warfarin from the wild-type VKOR simulation at 80 ns, showing that the RMSD for the warfarin-less VKOR structure rapidly relaxed in the direction of the reference structure. Warfarin retains its T-shaped stacking interaction with Y139 in the wild-type VKOR (**Figure 4B**), however, it loses the interaction and escapes from the binding pocket in the Y139A mutant (**Figure 4C**). The free phenyl ring of warfarin is positioned outside of VKOR's TM helices and forms hydrophobic interactions with a lipid molecule in the environment (**Supplemental Figure 2B**). These results strongly suggest that the aromatic ring of residue Y139, which enables the complex T-shaped stacking interactions, is the critical moiety for warfarin binding. Surface representations of the warfarin-binding pockets of VKOR and the Y139A mutant with warfarin are shown in **Supplemental Figure 3**.

Y25 and A26 interact with Y139 to stabilize warfarin binding in VKOR

When warfarin binds to VKOR, we initially observed that Y139 interacts with Y25 through water molecules from the environment via a hydrogen-bond network (**Figure 4D)**. After 24 ns

unconstrained conventional MD simulation, the relative configurations of Y25, Y139, and warfarin are somewhat changed - TM1 has rotated counter-clockwise, causing Y25 to move apart from Y139 and A26 to face toward Y139. A new hydrogen-bond network is observed in which Y139 interacts with both Y25 and A26 (backbone) via water molecules (**Figure 4E**); this network stabilizes warfarin binding to VKOR. To explore the contribution of A26 to warfarin binding, we performed the same MD simulation for the naturally occurring warfarin-resistant A26T mutant[35] in the presence of warfarin as we did for the Y139A mutant. Unexpectedly, the RMSD value for the A26T mutant increases to 2.5 Å at ~60 ns and then gradually moves toward the value of wild-type VKOR (**Supplemental Figure 4**). The RMSD value of A26T stabilizes similarly to that of the wild-type simulation beyond 200 ns (data not shown). This stability is apparently enabled by the formation of a direct hydrogen-bond between the hydroxyl groups of A26T and Y139, which stabilizes the warfarin-binding pocket (**Figure 4F**). This result suggests that the naturally occurring warfarin-resistant A26T mutant should have a similar warfarin sensitivity as wild-type VKOR.

Validation of the identified warfarin binding residues in physiological conditions

To experimentally evaluate our MD simulation results in physiological conditions, we mutated each of the identified residues critical to warfarin binding, as we did in the MD simulation. We then examined the warfarin-binding affinity of these mutants in a cellular environment[29]. **Figure 5A** shows that mutating these residues (Y25, A26 and Y139) has only a minor effect on VKOR activity. However, warfarin resistance of the Y139A mutant increases 284-fold (**Figure 5B** and **Supplemental Table 2**), suggesting that the warfarin-binding affinity is significantly reduced. This result is consistent with our MD simulation result, which shows that the Y139A mutant has significantly lower RMSD values and that warfarin eventually escapes from the binding pocket (**Figure 4A and 4C**). Additionally, the warfarin resistance of the Y25A mutant increased 24.3-fold **(Figure 5C**), which agrees with a recent

finding that the Y25 mutation is the causative mutation in the warfarin-resistant rat[36]. Nevertheless, mutating Y25 has significantly less effect on warfarin resistance than mutating Y139 (24.3-fold vs. 284-fold), suggesting that Y25 contributes less to warfarin binding than Y139. This, again, agrees with our MD simulation results, which indicate that Y25 does not directly interact with warfarin, but instead stabilizes the initial structure of VKOR by interacting with Y139 (**Figure 4D**).

The A26T mutation has been identified as a warfarin-resistant mutation in a patient who requires a high dose of phenprocoumon (4-hydroxycoumarin derivative similar to warfarin) to reach the desired anticoagulation effect[35]. However, our cell-based warfarin resistance results show that the A26T mutant has similar warfarin sensitivity as wild-type VKOR (**Figure 5D**). This result is again consistent with our MD simulation result in that the A26T mutant, with its warfarin binding site stabilized by forming a hydrogen-bond between A26T and Y139 (**Figure 4F**), has a similar RMSD profile as VKOR (**Supplemental Figure 4**). Therefore, the A26T mutation appears not to be the causative mutation for the warfarin-resistant phenotype of the reported patient.

Warfarin is a reversible inhibitor of VKOR

Our MD simulation results show that much of the distortion to VKOR's structure caused by warfarin binding can be restored instantaneously by removing warfarin from the VKOR/warfarin complex (**Figure 4A**). Likewise, the action of warfarin binding to the Y139A mutant appears to also support a reversible inhibition mechanism (**Figure 4C**). This agrees with the notion that warfarin is a reversible inhibitor of VKOR[23,24,37]. However, an irreversible inhibition mechanism has also previously been proposed for warfarin's inhibition of VKOR[20,21]. To distinguish warfarin's inhibition mechanism, we examined the effect of warfarin on the apparent Vmax of VKOR at different VKOR concentrations using our cell-based assay (VKOR concentrations were controlled by seeding different cell numbers in the cell culture plate as described in Methods section)[38]. The plotted lines of apparent

Vmax versus VKOR concentrations in the presence of warfarin have smaller slopes than the control line (without warfarin) (**Figure 5E**); all lines meet near the origin. This result suggests that warfarin's inhibition of VKOR is a reversible inhibition[39] (**Supplemental Note**, Distinguish between reversible and irreversible inhibitions). This reversible inhibition mechanism is further confirmed by the removal of warfarin from the warfarin/VKOR complex, as in the MD simulation. More than 70% of warfarin-inactivated VKOR activity can be restored by washing off the warfarin-inactivated VKOR containing microsomes (**Figure 5F**). Together, these results suggest that warfarin is a reversible inhibitor of VKOR, a finding that is consistent with our MD simulation results.

Proposed warfarin binding residues and vitamin K binding site in VKOR

Mutations of several residues in VKOR result in warfarin resistance. These residues are proposed as warfarin binding residues and their locations are assumed to be close to or within the vitamin K binding site[16,25,35,40]. It has been proposed that warfarin and vitamin K compete to bind to residue F55[25]. Residue F55 is located within a conserved region with several successive "small-XXX-small" motifs (the two small residues typically are glycine, but also could be alanine or serine) (**Figure 6A**), which is important for promoting membrane protein helix-helix interaction and membrane protein folding[41,42]. The third residues of the XXX sequences in these motifs are conserved aromatic residues, including F55, W59, and F63. These aromatic residues are located approximately on the same face of an alpha-helix of the peptide. To explore the possible role of these aromatic residues in VKOR, we mutated each of these residues to alanine and examined their effect on warfarin and vitamin K binding. **Figure 6B** shows that mutating these residues has only a minor effect on VKOR activity (vitamin K binding). However, these mutations dramatically decrease VKOR's warfarin-binding affinity; warfarin sensitivity of these mutants decreased from ~13-fold to ~600-fold compared to that of the wild-type enzyme (**Figures 6C** and **6D**). These results suggest that the "small-XXX-small" sequences in VKOR

significantly contribute to warfarin binding, but not to vitamin K binding. It also suggests that the proposed warfarin binding residues in VKOR do not necessarily comprise the vitamin K binding site.

Discussion

VKOR is the target of warfarin - the most widely used oral anticoagulant. Genetic variations in VKOR significantly affect warfarin's clinical dosages, making it difficult to achieve the desired anticoagulation effect[43]. About thirty missense mutations in the VKOR gene have been identified in patients requiring high doses of warfarin to reach the desired anticoagulation (**Supplemental Table 3**). These mutations are referred to as warfarin-resistant mutations. However, it is not clear why most of these mutations significantly decrease the affinity of warfarin-binding, but do not affect vitamin K binding[29,40]. Therefore, a detailed structure-guided understanding of how warfarin targets VKOR in its native milieu is not only essential for clarifying the mechanism of action, but also provides important clues into warfarin dosage management and to the possible development of new anticoagulant drugs.

The binding of a substrate or inhibitor to an enzyme is a dynamic process that often alters the enzyme's structure[44,45]. To better understand the dynamic structural details of VKOR upon warfarin binding, we used MD simulation, a powerful tool for studying protein dynamics[46], to explore the process of warfarin binding to VKOR. Our results show that the hydrophobic interactions between the TM helices that stabilize VKOR's structure are sequentially weakened to allow warfarin to access its bindings site (**Figure 3**). When warfarin reaches its binding pocket, it forms a stabilized interaction with Y139 through the complex T-shaped π-π stacking interaction. This interaction is further confirmed by unconstrained MD simulations (**Figure 4**) and by cell-based functional studies of the Y139A mutant (**Figure 5**).

The T-shaped stacking configuration between warfarin and Y139 can happen only in the three-TM model of VKOR, not the four-TM model[16,47]. In the three-TM model, residue Y139 and the

$C_{132}XXC_{135}$ active site motif, together with the three TM helices, form a hydrophobic binding pocket (**Supplemental Figure 3**). This pocket is consistent with the hydrophobic characteristics of the enzyme's substrate/inhibitor. Additionally, in the three-TM model, the distribution of the charged residue flanking TM1 agrees with the "positive-inside rule"[48-51] (**Figure 7A** and **7B**), a dominant factor that affects the orientation of a given TM helix of membrane proteins. Furthermore, four tryptophan residues and one cytoplasmic lysine residue are located at the membrane's bilayer interface of the three-TM model of VKOR (**Figure 7C),** serving as anchoring residues to fix the TM helix within the lipid bilayer[52-55]. These membrane interfacial residues play an important role in controlling the membrane protein's stability and function[56]. Of the six membrane interfaces, only the N-terminus of TM3, near the enzyme's active site, does not have a characteristic interface-defining residue. This could be related to this local sequence being involved in the substrate binding and/or product releasing.

All the above defining features, however, appear to be inconsistent with the four-TM model of human VKOR derived from the structure of *Syn*-VKOR (**Supplemental Note**, The differences between human VKOR and its bacterial homologue). The orientation of TM1 in the four-TM model is especially at odds with the "positive-inside rule". However, the orientation of TM1 of *Syn*-VKOR in the four-TM structure agrees with the "positive-inside rule" (**Figure 7A**). In general, the three-TM model for human VKOR and the four-TM model for *Syn*-VKOR appear to fit most of the membrane protein topology determinants. The controversy concerning the membrane topology of human VKOR basically arises from the direct application of the human VKOR sequence to the four-TM *Syn*-VKOR topological structure.

Our MD simulation results show that when warfarin binds to VKOR, it causes a modest reversible distortion of VKOR's architecture but does not disrupt the overall three-TM structure. This observed conformational change of VKOR's architecture involves a large number of residues; mutating any of these residues could affect warfarin binding without affecting vitamin K binding. As

we observed, mutating residues Y25, F55, W59, F63, and Y139 significantly increased warfarin resistance, but only had a minor effect on VKOR activity (**Figures 5** and **6**). Additionally, residue L128, like Y139, appears to be another "hot-spot" for the naturally occurring warfarin-resistant mutations (**Supplemental Table 3**). Mutating L128 significantly increased warfarin resistance (~30-fold) but did not affect VKOR activity[29,40]. This again is consistent with our MD simulation results showing that L128 interacts with L15 to stabilize VKOR's structure and controls the opening and closing of the putative warfarin-binding pocket (**Figure 3**). Therefore, our model sucessfully explains why most of the warfarin-resistant mutants have normal VKOR activity, which agrees with the non-bleeding phenotypes of patients carrying these mutations.

Our results from both the MD simulation and the cell-based activity assay study suggest that the naturally occurring A26T mutation is not the causative mutation for the warfarin-resistant phenotype. These results are consistent with previous studies showing that not all warfarin-resistant VKOR mutations identified in patients are associated with warfarin-resistant VKOR activity[29,37]. It suggests that factors other than VKOR could play important roles in the warfarin-resistant phenotype. For example, in addition to clinical variables, genetic variation of cytochrome P450 2C9 (a warfarin metabolism enzyme), has also been strongly associated with warfarin-resistant phenotype[57]. The general consistency of our MD simulation results, along with the cell-based experimental data, not only helps us to understand the mechanism of warfarin inhibtion of VKOR, but also provides important clues into the explanation of warfarin-resistant clinical phenotypes and into designing safer anticoagulant drugs for treating disorders involving vitamin K metabolism.

Acknowledgements

We thank Dr. J.Y. Shim for technical assistance on the parameterization of warfarin. This work was supported by grant HL131690 from the National Institutes of Health, USA (to J.K.T. and D.W.S.) and the National Research Foundation of Korea (NRF) funded by the Ministry of Education (2015R1D1A1A01061125) (to S.W.)

Authorship Contributions

S.W., D.W.S., J.K.T., and L.G.P. conceived the studies. S.W. performed MD simulation and analyzed the data. X.C. and D.Y.J. performed cell-based VKOR function studies and analyzed the data. X.C. performed enzyme kinetics study and VKOR endogenous cysteine PEGylation. J.K.T. performed immunofluorescence confocal microscopy study. S.W., J.K.T., and L.G.P. wrote the manuscript.

Conflict of Interest Disclosures

The authors declare no competing financial interests.

References

1. Zirlik A, Bode C. Vitamin K antagonists: relative strengths and weaknesses vs. direct oral anticoagulants for stroke prevention in patients with atrial fibrillation. J Thromb Thrombolysis. 2017;43(3):365-379.

2. Johnson ME, Lefevre C, Collings SL, et al. Early real-world evidence of persistence on oral anticoagulants for stroke prevention in non-valvular atrial fibrillation: a cohort study in UK primary care. BMJ Open. 2016;6(9):e011471.

3. Jacobson A. Is there a role for warfarin anymore? Hematology Am Soc Hematol Educ Program. 2012;2012:541-546.

4. Di Minno A, Frigerio B, Spadarella G, et al. Old and new oral anticoagulants: Food, herbal medicines and drug interactions. Blood Rev. 2017;31(4):193-203.

5. Arwood MJ, Deng J, Drozda K, et al. Anticoagulation endpoints with clinical implementation of warfarin pharmacogenetic dosing in a real-world setting: A proposal for a new pharmacogenetic dosing approach. Clin Pharmacol Ther. 2017;101(5):675-683.

6. Stafford DW. The vitamin K cycle. J Thromb Haemost. 2005;3(8):1873-1878.

7. Jin DY, Tie JK, Stafford DW. The conversion of vitamin K epoxide to vitamin K quinone and vitamin K quinone to vitamin K hydroquinone uses the same active site cysteines. Biochemistry. 2007;46(24):7279-7283.

8. Wajih N, Sane DC, Hutson SM, Wallin R. Engineering of a recombinant vitamin K-dependent gamma-carboxylation system with enhanced gamma-carboxyglutamic acid forming capacity:

evidence for a functional CXXC redox center in the system. J Biol Chem. 2005;280(11):10540-10547.

9. Schwarz R, Seibel PN, Rahmann S, et al. Detecting species-site dependencies in large multiple sequence alignments. Nucleic Acids Res. 2009;37(18):5959-5968.

10. Pelz HJ, Rost S, Hunerberg M, et al. The genetic basis of resistance to anticoagulants in rodents. Genetics. 2005;170(4):1839-1847.

11. Oldenburg J, Bevans CG, Muller CR, Watzka M. Vitamin K epoxide reductase complex subunit 1 (VKORC1): the key protein of the vitamin K cycle. Antioxid Redox Signal. 2006;8(3-4):347-353.

12. Van Horn WD. Structural and functional insights into human vitamin K epoxide reductase and vitamin K epoxide reductase-like1. Crit Rev Biochem Mol Biol. 2013;48(4):357-372.

13. Cao Z, van Lith M, Mitchell LJ, Pringle MA, Inaba K, Bulleid NJ. The membrane topology of vitamin K epoxide reductase is conserved between human isoforms and the bacterial enzyme. Biochem J. 2016;473(7):851-858.

14. Tie JK, Jin DY, Stafford DW. Human vitamin K epoxide reductase and its bacterial homologue have different membrane topologies and reaction mechanisms. J Biol Chem. 2012;287(41):33945-33955.

15. Tie JK, Nicchitta C, von Heijne G, Stafford DW. Membrane topology mapping of vitamin K epoxide reductase by in vitro translation/cotranslocation. J Biol Chem. 2005;280(16):16410-16416.

16. Li W, Schulman S, Dutton RJ, Boyd D, Beckwith J, Rapoport TA. Structure of a bacterial homologue of vitamin K epoxide reductase. Nature. 2010;463(7280):507-512.

17. Wu S, Tie JK, Stafford DW, Pedersen LG. Membrane topology for human vitamin K epoxide reductase. J Thromb Haemost. 2014;12(1):112-114.

18. Wu S, Liu S, Davis CH, Stafford DW, Kulman JD, Pedersen LG. A hetero-dimer model for concerted action of vitamin K carboxylase and vitamin K reductase in vitamin K cycle. J Theor Biol. 2011;279(1):143-149.

19. Rishavy MA, Usubalieva A, Hallgren KW, Berkner KL. Novel insight into the mechanism of the vitamin K oxidoreductase (VKOR): electron relay through Cys43 and Cys51 reduces VKOR to allow vitamin K reduction and facilitation of vitamin K-dependent protein carboxylation. J Biol Chem. 2011;286(9):7267-7278.

20. Fasco MJ, Principe LM. R- and S-Warfarin inhibition of vitamin K and vitamin K 2,3-epoxide reductase activities in the rat. J Biol Chem. 1982;257(9):4894-4901.

21. Silverman RB. Model studies for a molecular mechanism of action of oral anticoagulants. J Am Chem Soc. 1981;103(13):3910-3915.

22. Thijssen HH, Baars LG, Vervoort-Peters HT. Vitamin K 2,3-epoxide reductase: the basis for stereoselectivity of 4-hydroxycoumarin anticoagulant activity. Br J Pharmacol. 1988;95(3):675-682.

23. Matagrin B, Hodroge A, Montagut-Romans A, et al. New insights into the catalytic mechanism of vitamin K epoxide reductase (VKORC1) - The catalytic properties of the major mutations of rVKORC1 explain the biological cost associated to mutations. FEBS Open Bio. 2013;3:144-150.

24. Lasseur R, Longin-Sauvageon C, Videmann B, Billeret M, Berny P, Benoit E. Warfarin resistance in a French strain of rats. J Biochem Mol Toxicol. 2005;19(6):379-385.

25. Czogalla KJ, Biswas A, Honing K, et al. Warfarin and vitamin K compete for binding to Phe55 in human VKOR. Nat Struct Mol Biol. 2017;24(1):77-85.

26. Timson DJ. Dicoumarol: a drug which hits at least two very different targets in vitamin K metabolism. Curr Drug Targets. 2017;18(5):500-510.

27. Howe V, Brown AJ. Determining the Topology of Membrane-Bound Proteins Using PEGylation. Methods Mol Biol. 2017;1583:201-210.

28. Bogdanov M. Mapping of Membrane Protein Topology by Substituted Cysteine Accessibility Method (SCAM). Methods Mol Biol. 2017;1615:105-128.

29. Tie JK, Jin DY, Tie K, Stafford DW. Evaluation of warfarin resistance using transcription activator-like effector nucleases-mediated vitamin K epoxide reductase knockout HEK293 cells. J Thromb Haemost. 2013;11(8):1556-1564.

30. Labay V, Weichert RM, Makishima T, Griffith AJ. Topology of transmembrane channel-like gene 1 protein. Biochemistry. 2010;49(39):8592-8598.

31. Jin DY, Vermeer C, Stafford DW, Tie JK. Splice-Site Mutation of Exon 3 Deletion in the Gamma-Glutamyl Carboxylase Gene Causes Inactivation of the Enzyme. J Invest Dermatol. 2016;136(11):2314-2317.

32. Hsia CK. Biochemical and Mechanistic Studies of the Interactions Between Vitamin K Antagonists and Vitamin K Epoxide Reductase. PhD thesis. 2012;Chapter 3(An In Vitro

Investigation of VKOR Inhibitory Mechanisms by Vitamin K Antagonists in Bovine Liver Microsomes):University of Washington, Seattle, WA.

33. Lu H, Isralewitz B, Krammer A, Vogel V, Schulten K. Unfolding of titin immunoglobulin domains by steered molecular dynamics simulation. Biophys J. 1998;75(2):662-671.

34. Izrailev S, Stepaniants S, Balsera M, Oono Y, Schulten K. Molecular dynamics study of unbinding of the avidin-biotin complex. Biophys J. 1997;72(4):1568-1581.

35. Watzka M, Geisen C, Bevans CG, et al. Thirteen novel VKORC1 mutations associated with oral anticoagulant resistance: insights into improved patient diagnosis and treatment. J Thromb Haemost. 2011;9(1):109-118.

36. Goulois J, Chapuzet A, Lambert V, et al. Evidence of a target resistance to antivitamin K rodenticides in the roof rat Rattus rattus: identification and characterisation of a novel Y25F mutation in the Vkorc1 gene. Pest Manag Sci. 2016;72(3):544-550.

37. Hodroge A, Matagrin B, Moreau C, et al. VKORC1 mutations detected in patients resistant to vitamin K antagonists are not all associated with a resistant VKOR activity. J Thromb Haemost. 2012;10(12):2535-2543.

38. Tie JK, Jin DY, Straight DL, Stafford DW. Functional study of the vitamin K cycle in mammalian cells. Blood. 2011;117(10):2967-2974.

39. Segel IH. Enzyme Kinetics: Behavior and Analysis of Rapid Equilibrium and Steady-State Enzyme Systems. Wiley-Interscience. 1993.

40. Shen G, Cui W, Zhang H, et al. Warfarin traps human vitamin K epoxide reductase in an intermediate state during electron transfer. Nat Struct Mol Biol. 2017;24(1):69-76.

41. Teese MG, Langosch D. Role of GxxxG motifs in transmembrane domain interactions. Biochemistry. 2015;54(33):5125-5135.

42. Russ WP, Engelman DM. The GxxxG motif: a framework for transmembrane helix-helix association. J Mol Biol. 2000;296(3):911-919.

43. Zineh I, Pacanowski M, Woodcock J. Pharmacogenetics and coumarin dosing--recalibrating expectations. N Engl J Med. 2013;369(24):2273-2275.

44. Weikl TR, Hemmateenejad B. How conformational changes can affect catalysis, inhibition and drug resistance of enzymes with induced-fit binding mechanism such as the HIV-1 protease. Biochim Biophys Acta. 2013;1834(5):867-873.

45. Teague SJ. Implications of protein flexibility for drug discovery. Nature Reviews Drug Discovery. 2003;2(7):527-541.

46. Salsbury FR, Jr. Molecular dynamics simulations of protein dynamics and their relevance to drug discovery. Curr Opin Pharmacol. 2010;10(6):738-744.

47. Lewis BC, Nair PC, Heran SS, et al. Warfarin resistance associated with genetic polymorphism of VKORC1: linking clinical response to molecular mechanism using computational modeling. Pharmacogenet Genomics. 2016;26(1):44-50.

48. Baker JA, Wong WC, Eisenhaber B, Warwicker J, Eisenhaber F. Charged residues next to transmembrane regions revisited: "Positive-inside rule" is complemented by the "negative inside depletion/outside enrichment rule". BMC Biol. 2017;15(1):66.

49. Dowhan W, Bogdanov M. Lipid-dependent membrane protein topogenesis. Annu Rev Biochem. 2009;78:515-540.

50. White SH, von Heijne G. The machinery of membrane protein assembly. Curr Opin Struct Biol. 2004;14(4):397-404.

51. von Heijne G. Control of topology and mode of assembly of a polytopic membrane protein by positively charged residues. Nature. 1989;341(6241):456-458.

52. de Jesus AJ, Allen TW. The role of tryptophan side chains in membrane protein anchoring and hydrophobic mismatch. Biochim Biophys Acta. 2013;1828(2):864-876.

53. Schiffer M, Chang CH, Stevens FJ. The functions of tryptophan residues in membrane proteins. Protein Eng. 1992;5(3):213-214.

54. Ridder AN, Morein S, Stam JG, Kuhn A, de Kruijff B, Killian JA. Analysis of the role of interfacial tryptophan residues in controlling the topology of membrane proteins. Biochemistry. 2000;39(21):6521-6528.

55. de Planque MR, Kruijtzer JA, Liskamp RM, et al. Different membrane anchoring positions of tryptophan and lysine in synthetic transmembrane alpha-helical peptides. J Biol Chem. 1999;274(30):20839-20846.

56. Killian JA, von Heijne G. How proteins adapt to a membrane-water interface. Trends Biochem Sci. 2000;25(9):429-434.

57. Misasi S, Martini G, Paoletti O, et al. VKORC1 and CYP2C9 polymorphisms related to adverse events in case-control cohort of anticoagulated patients. Medicine (Baltimore). 2016;95(52):e5451.

Figure Legends

Figure 1 Membrane topology of human VKOR. (A) The proposed three-TM (based on reference 15) and four-TM (based on reference 16) topology models of human VKOR. Cysteine residues (C43, C51, C85, and C96) in the disputed loop sequence are marked in red. Cysteine residues (C16, C132, and C135) located within the TM helices are not shown. The loop sequence (A34-W59) specifically recognized by a VKOR antibody is marked green in the three-TM model and blue in the four-TM model. (**B**) Localization of the disputed loop sequence of human VKOR by immunofluorescence confocal microscopy in live mammalian cells. COS-7 cells expressing wild-type human VKOR were either selectively or fully permeabilized with digitonin or Triton X-100, respectively. Cytoplasmic proteins are accessible to antibody staining after selective permeabilization with digitonin, while ER lumen proteins are accessible for staining after full permeabilization with Triton X-100. Cells were co-immunostained with anti-VKOR (red) and anti-PDI (green) antibodies (top panel) or with anti-VKOR (red) and anti-tubulin (green) antibodies (bottom panel). The cell nucleus was stained by Hoechst 33342 (blue). (**C**) PEGylation of the cytoplasmic-accessible cysteines of VKOR with a membrane-impermeable maleimide polyethylene glycol (mPEG-MAL-5000). C-terminal FLAG tagged VKOR or its C43/51A mutant was stably expressed in HEK293 cells. Intact microsomes were prepared and labeled with mPEG-MAL-5000 with/without Triton X-100 permeabilization. VKOR bands were visualized by Western blot analysis. (**D**) Cell-based activity assay of VKOR and its C43/51A mutant. Data are presented as mean±SD (n=3).

Figure 2 MD simulation of warfarin binding to VKOR. (**A**) The initial position of warfarin and the three-TM VKOR in POPE lipid bilayer in the ionic water environment. For clarity, water molecules and ions are not shown. Warfarin was added to the ER lumen of VKOR (structure of the last snapshot of the 62 ns simulation according to reference 17), and equilibrated for 40 ns using unconstrained conventional MD simulation. (**B**) Snapshots of the steered MD simulation of warfarin accessing the putative binding site of VKOR during 448 ps. For clarity, water, ions, and lipids molecules are not shown. Key residues, encountered during warfarin accessing the binding site in VKOR, are labeled and displayed using stick diagrams.

Figure 3 Sequential binding pocket opening when warfarin accesses its binding site. The profile of the minimum distances between the hydrophobic paired leucine residues (L15:L111, L15:L128, and L22:L105) that help sustain a stable VKOR structure are recorded during the 448 ps steered MD simulation (bottom). Snapshots of warfarin inside VKOR at the indicated time points are shown (inserts). Key residues, encountered during warfarin's accessing the binding site in VKOR, are labeled and displayed using stick diagrams. Minimum distances between paired lysine residues are labeled.

Figure 4 Unconstrained MD simulation of warfarin binding to VKOR, Y139A, and A26T mutants. (**A**) The backbone RMSD profiles of VKOR (red) and the Y139A mutant (blue) during the 200 ns unconstrained MD simulation. The green curve shows the backbone RMSD profile of wild-type VKOR when warfarin is removed at the 80 ns time point and the structure is re-equilibrated before additional simulation. (**B**) Warfarin binding to wild-type VKOR at the last snapshot of the 200 ns unconstrained MD simulation. A T-shaped π-π

stacking interaction between warfarin and Y139 is shown (nearest carbon-carbon distance of 3.36 Å). (**C**) Warfarin binding to the Y139A mutant at the last snapshot of the 200 ns unconstrained MD simulation. Warfarin drifts away from its initial site. (**D**) Configuration of Y25, Y139, and warfarin at the last snapshot of the 448 ps steered MD simulation. Y25 stabilizes Y139 by forming a hydrogen bond network via water molecules from the environment. (**E**) Warfarin-binding pocket at the 24 ns snapshot of the unconstrained conventional MD simulation. Y139 was stabilized by forming a new hydrogen bond network via water molecules with the backbone of A26. (**F**) Configuration of the warfarin-binding pocket of the A26T mutant at 200 ns snapshot of the unconstrained conventional MD simulation. Y139 was stabilized by directly forming a hydrogen bond with A26T.

Figure 5 Functional study of VKOR and its mutants. (**A**) Cell-based activity assay of VKOR and its mutants. Data are presented as mean±SD (n=3). Warfarin resistance study of the Y139A mutant (**B**), the Y25A mutant (**C**), and the A26T mutant (**D**) were performed by culturing the VKOR/VKORC1L1-knockout FIXgla-PC/HEK293 reporter cells expressing the individual mutant with 5 μM KO containing increasing concentrations of warfarin. Warfarin resistance, as determined by the half-maximal inhibition concentration (IC_{50}), is available in **Supplemental Table 2**. (**E**) The response of apparent Vmax to VKOR concentrations in the presence and absence of warfarin. Apparent Vmax was determined under different enzyme concentrations, with 0 nM, 2 nM, and 10 nM warfarin. VKOR concentrations were controlled by seeding different numbers of the reporter cells into the multi-well cell culture plate. Since the reporter cell line was derived from a single cell colony, we assume that each individual cell has a similar expression level of the endogenous VKOR and VKOR concentration is

proportional to the cell numbers. (**F**) Removal of warfarin from the VKOR-warfarin complex. VKOR containing microsomes were incubated with 30 μM warfarin on ice for 30 minutes; warfarin was then removed by dilution and ultracentrifugation for activity assay. VKOR: VKOR containing microsomes; VKOR+warfarin: VKOR-containing microsomes incubated with 30 μM warfarin; Wash: warfarin treated VKOR containing microsomes after wash.

Figure 6 Functional study of the aromatic residues in the small-XXX-small motifs of the loop sequence in VKOR. (**A**) Multiple sequence alignment of VKOR near the small-XXX-small motifs of the loop sequence. Amino acid sequences of VKOR from widely divergent species were aligned by CLUSTAL W. Conserved aromatic residues are indicated by numbers according to the position of amino acid residues in the human VKOR sequence. (**B**) Cell-based activity assay of the aromatic residue mutants of VKOR. (**C**) Warfarin resistance study of the aromatic residue mutants of VKOR, performed as described in the legend for **Figure 5**. (**D**) Normalized warfarin resistance of the aromatic residue mutants of VKOR. Warfarin sensitivity of wild-type VKOR was normalized to 1. Warfarin resistance, as determined by the half-maximal inhibition concentration (IC_{50}), is available in **Supplemental Table 2**.

Figure 7 Membrane protein topology determinants and the proposed three-TM membrane topology for human VKOR. (**A**) Charged residue distribution flanking TM1 of human VKOR and *Syn*-VKOR. Positively charged residues are indicated by red arrow-heads and negatively charged residues are indicated by filled green circles. Net charges flanking TM1 of both proteins are indicated. Boxed sequences represent the proposed TM1 according to references 15 and 16. Sequence alignment was adapted from reference 16. (**B**) Distribution of

charged residues flanking TM1 in the proposed three-TM structure of human VKOR. Positively and negatively charged residues are highlighted and labeled with single letter amino acid abbreviations. (**C**) Distribution of the membrane interfacial anchors in the proposed three-TM structure of human VKOR. Membrane interfacial residues and active site cysteine residues are highlighted and labeled with single letter amino acid abbreviations.

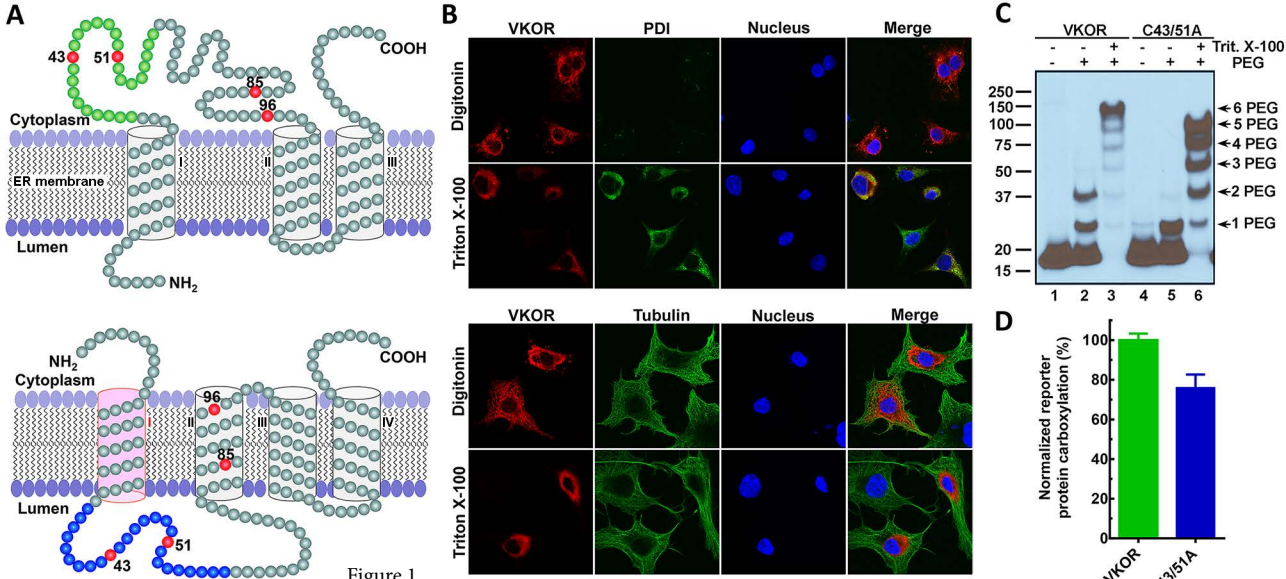
A
43
51
85
96
COOH
Cytoplasm
ER membrane
Lumen
NH2
I
II
III
IV
B
VKOR
PDI
Nucleus
Merge
Digitonin
Triton X-100
Tubulin
C
VKOR
C43/51A
Trit. X-100
PEG
250
150
100
75
50
37
20
15
6 PEG
5 PEG
4 PEG
3 PEG
2 PEG
1 PEG
1 2 3 4 5 6
D
Normalized reporter protein carboxylation (%)
100
80
60
40
20
0
VKOR
C43/51A

Figure 1

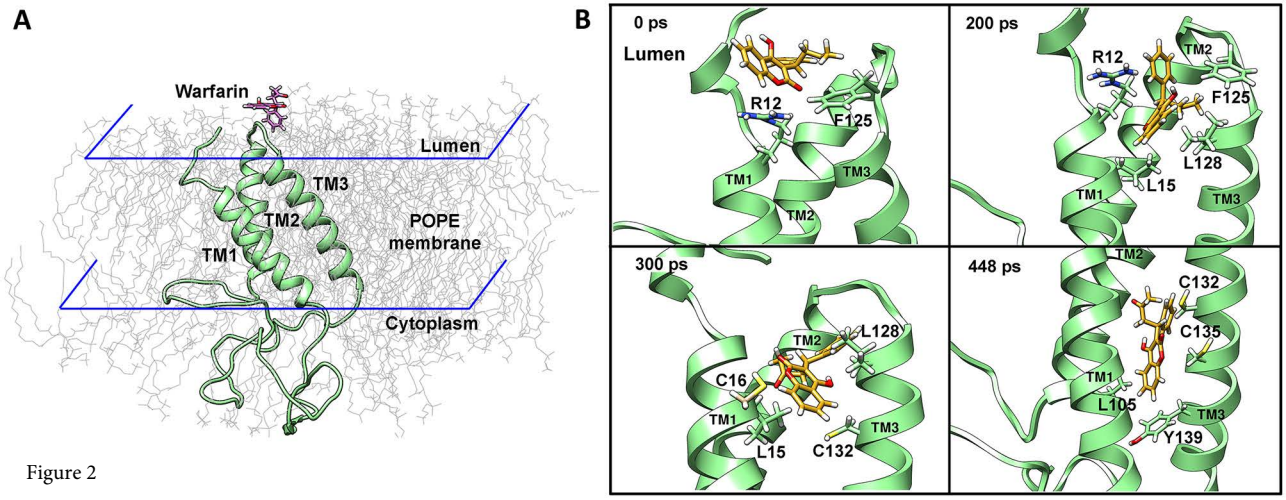
A
Warfarin
Lumen
TM3
TM2
TM1
POPE
membrane
Cytoplasm
B
0 ps
Lumen
R12
F125
TM1
TM3
TM2
200 ps
R12
TM2
F125
L128
L15
TM1
TM3
300 ps
L128
TM2
C16
TM1
L15
C132
TM3
448 ps
TM2
C132
C135
TM1
L105
TM3
Y139

Figure 2

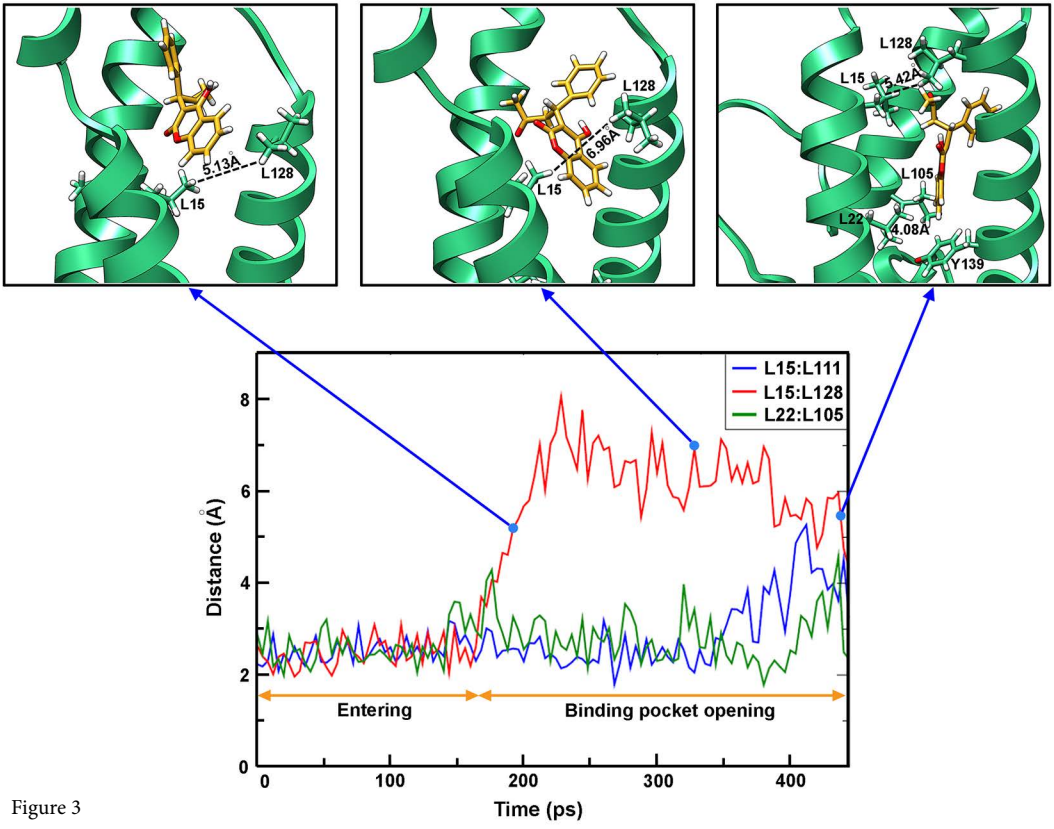
5.13Å
L128
L15
6.96Å
L128
L15
L128
L15
5.42Å
L105
L22
4.08Å
Y139
L15:L111
L15:L128
L22:L105
Distance (Å)
Time (ps)
Entering
Binding pocket opening
0
2
4
6
8
0
100
200
300
400

Figure 3

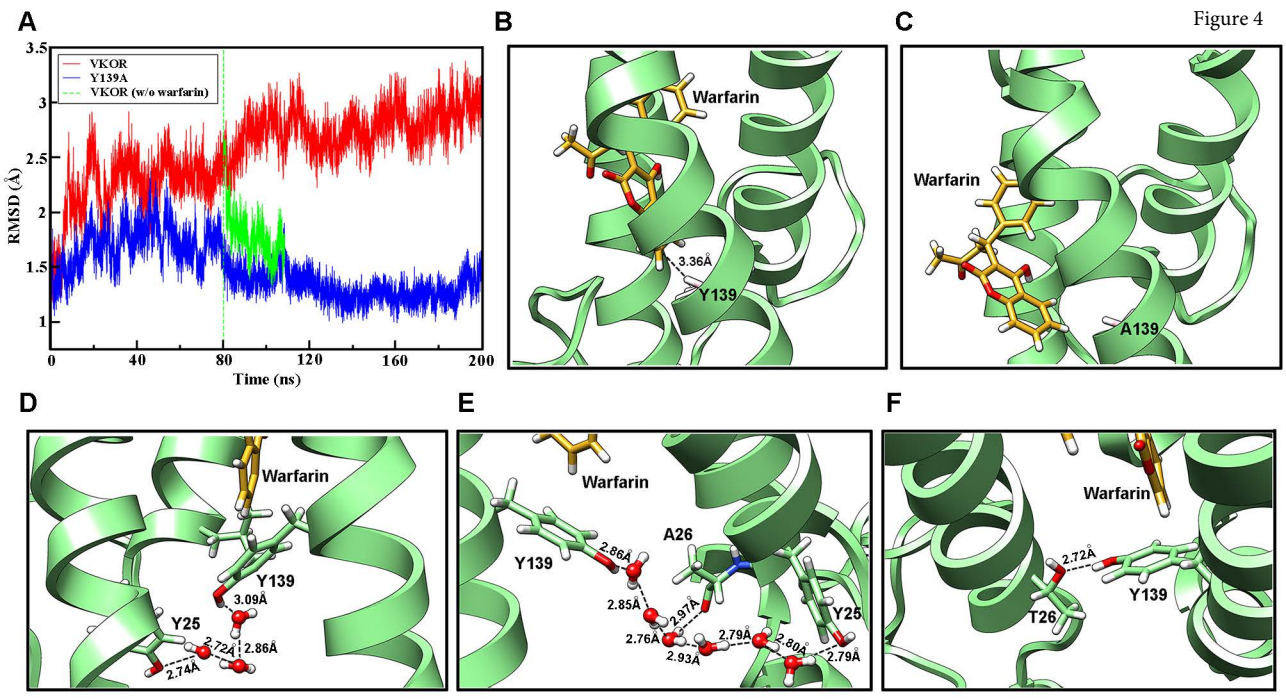
A
VKOR
Y139A
VKOR (w/o warfarin)
RMSD (Å)
Time (ns)
B
Warfarin
3.36Å
Y139
C
Warfarin
A139
D
Warfarin
Y139
3.09Å
Y25
2.72Å
2.86Å
2.74Å
E
Warfarin
Y139
2.86Å
A26
2.85Å
2.97Å
2.76Å
2.93Å
2.79Å
2.80Å
Y25
2.79Å
F
Warfarin
2.72Å
T26
Y139

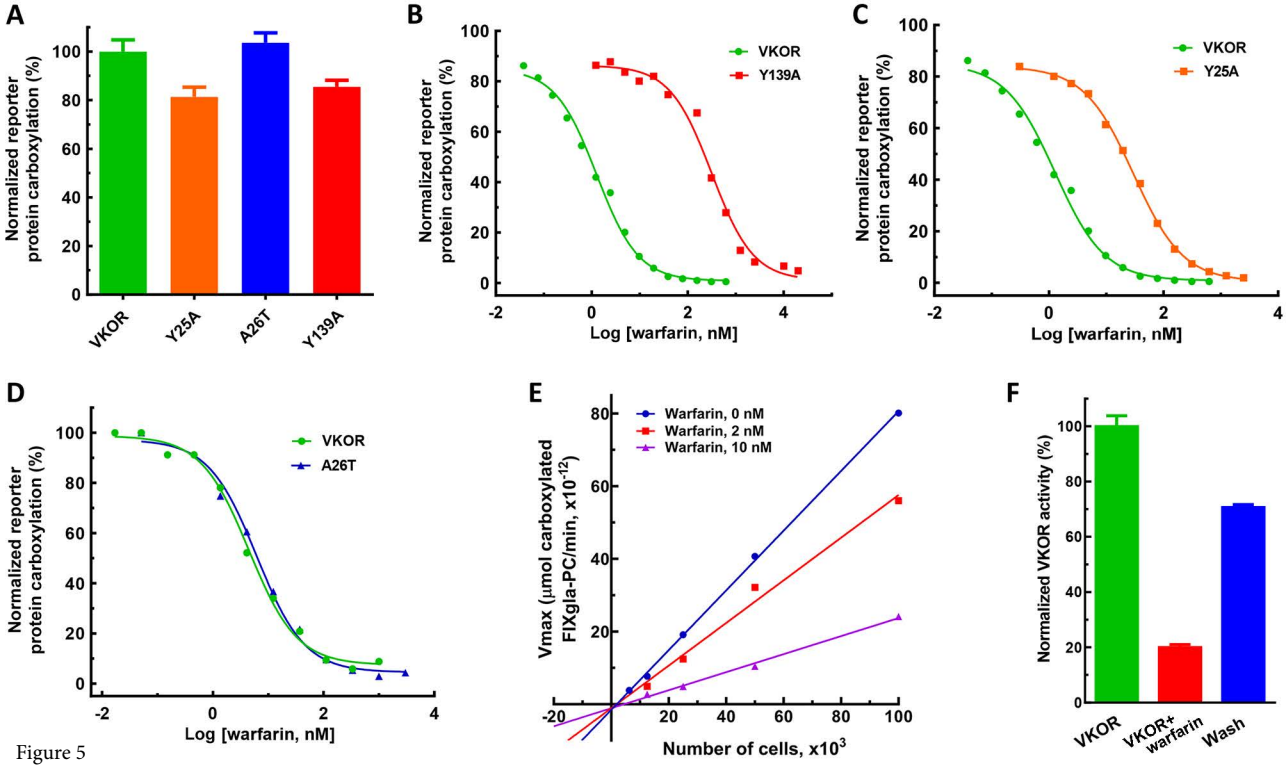
A
Normalized reporter protein carboxylation (%)
VKOR
Y25A
A26T
Y139A
B
Normalized reporter protein carboxylation (%)
VKOR
Y139A
Log [warfarin, nM]
C
Normalized reporter protein carboxylation (%)
VKOR
Y25A
Log [warfarin, nM]
D
Normalized reporter protein carboxylation (%)
VKOR
A26T
Log [warfarin, nM]
E
Warfarin, 0 nM
Warfarin, 2 nM
Warfarin, 10 nM
Vmax (µmol carboxylated FIXgla-PC/min, x10-12)
Number of cells, x103
F
Normalized VKOR activity (%)
VKOR
VKOR+ warfarin
Wash

Figure 5

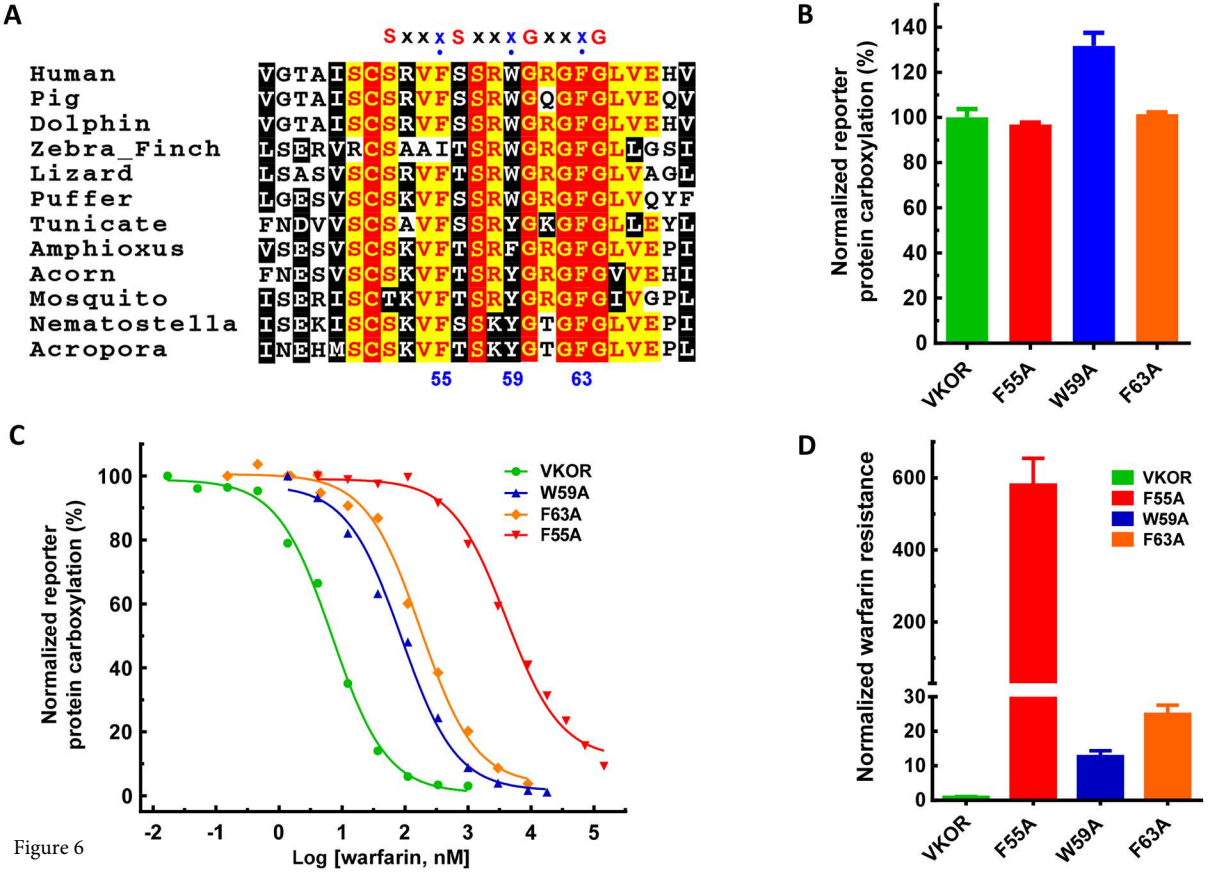
A
Sxxx S xxx G xxx G
Human VGTAISCSRVFSSRWGRGFGLVEHV
Pig VGTAISCSRVFSSRWGQGFGLVEQV
Dolphin VGTAISCSRVFSSRWGRGFGLVEHV
Zebra_Finch LSERVRCSAAITSRWGRGFGLLGSI
Lizard LSASVSCSRVFTSRWGRGFGLVAGL
Puffer LGESVSCSKVFSSRWGRGFGLVQYF
Tunicate FNDVVSCSAVFSSRYGKGFGLLEYL
Amphioxus VSESVSCSKVFTSRFGRGFGLVEPI
Acorn FNESVSCSKVFTSRYGRGFGVVEHI
Mosquito ISERISCTKVFTSRYGRGFGIVGPL
Nematostella ISEKISCSKVFSSKYGTGFGLVEPI
Acropora INEHMSCSKVFTSKYGTGFGLVEPL
55
59
63
B
Normalized reporter protein carboxylation (%)
0
20
40
60
80
100
120
140
VKOR
F55A
W59A
F63A
C
Normalized reporter protein carboxylation (%)
0
20
40
60
80
100
VKOR
W59A
F63A
F55A
-2
-1
0
1
2
3
4
5
Log [warfarin, nM]
D
Normalized warfarin resistance
0
10
30
200
400
600
VKOR
F55A
W59A
F63A

Figure 6

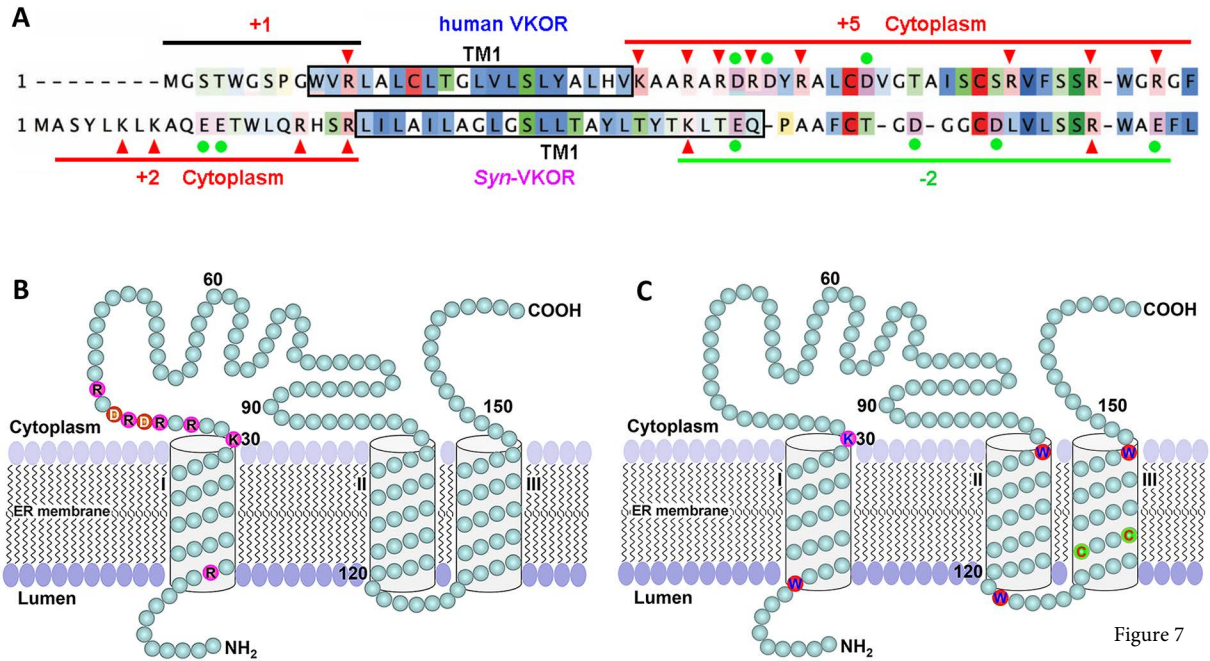
A
+1
human VKOR
TM1
+5
Cytoplasm
1 - - - - - - - - MGSTWGSPGWVRLALCLTGLVLSLYALHVKAARARDRDYRALCDVGTAISCSRVFSSR-WGRGF
1 MASYLKLKAQEETWLQRHSRLILAILAGLGSLLTAYLTYTKLTEQ-PAAFCT-GD-GGCDLVLSSR-WAEFL
TM1
+2
Cytoplasm
Syn-VKOR
-2
B
60
COOH
90
150
Cytoplasm
30
I
II
III
ER membrane
120
Lumen
NH2
C
60
COOH
90
150
Cytoplasm
30
I
II
III
ER membrane
120
Lumen
NH2

Figure 7

Prepublished online May 9, 2018;
doi:10.1182/blood-2018-01-830901

Warfarin and vitamin K epoxide reductase: a molecular accounting for observed inhibition

Sangwook Wu, Xuejie Chen, Da-Yun Jin, Darrel W. Stafford, Lee G. Pedersen and Jian-Ke Tie